06 Aug 2003

Modeling for the Control of the Laser Aided Manufacturing Process (LAMP)

Mallikharjuna R. Boddu

Vishnu P. Thayalan

Robert G. Landers
Missouri University of Science and Technology, landersr@mst.edu

Recommended Citation

M. R. Boddu et al., "Modeling for the Control of the Laser Aided Manufacturing Process (LAMP)," *Proceedings of the 14th Annual Solid Freeform Fabrication Symposium (2003, Austin, TX)*, pp. 186-195, University of Texas at Austin, Aug 2003.

Modeling for the Control of the Laser Aided Manufacturing Process (LAMP)

Mallikharjuna R. Boddu, Vishnu P. Thayalan, and Robert G. Landers

1870 Miner Circle, 211 Mechanical Engineering Building
Department of Mechanical and Aerospace Engineering and Engineering Mechanics
University of Missouri – Rolla, Missouri 65409
Phone: 573–341–4586
Email: {mallik,vishnu,landersr}@umr.edu

Reviewed, accepted August 19, 2003

ABSTRACT

Many state–of–the–art Rapid Prototyping (RP) technologies adopt lasers to fabricate 3–D solid parts by material deposition in layers. The ability of these RP technologies to control the process requires a thorough understanding of the process mechanics. This paper presents the analysis of an analytical, dynamic model explaining the complex phenomenon of Laser Aided Manufacturing Process (LAMP). The equilibrium of the dynamic model is analyzed and dynamic simulations are performed to determine its stability characteristics. This model forms the basis for the real–time control of the LAMP.

INTRODUCTION

Rapid prototyping (RP) is a valuable tool for the fabrication of 3D models. RP decreases the product development cycle by enabling the part to be built in hours instead of weeks directly from the CAD model by eliminating the intermediate step of die preparation. There are a variety of RP processes currently available. RP processes can be divided into those that are formative, subtractive, or additive. Additive–based RP is gaining importance due to its capability to build functional–gradient parts. Laser based RP is one such technology experiencing striding growth in the manufacturing industry since its introduction in the early 1980s. There are around 25 different laser based RP technologies practiced under different names such as stereolithography, Fused Deposition Modeling (FDM), Direct Metal Deposition (DMD), Laser Engineered Net Shaping (LENS), etc. [Steen, 1998]. All of these methods concentrate on building 3D functional parts with minimum cost and in the least amount of time with required tolerance and surface finish.

Laser Aided Manufacturing Process (LAMP) is a technology that is being developed at the University of Missouri–Rolla to fabricate high–resolution 3D parts of arbitrary shapes directly from CAD models with the ability for the user to define material composition throughout the building process. LAMP is based on the simple technique of adding layers until a 3D metal prototype is obtained by selective cladding point–by–point and layer–by–layer [Boddu *et al.,* 2001]. The dimensional accuracy of the part is maintained from the initial stages by allowing the deposition and milling operations to be performed in shifts throughout the part building process, but the scientific challenge lies in the ability of the LAMP system to precisely fabricate the part by minimizing the post deposition operation. This depends on the capability of the system to control the LAMP process in real–time. Previous efforts have been made by many authors in designing a control system to regulate the laser metal deposition process. But these efforts have been limited to regulating few of the process parameters due to the complexities and limitations

involved in understanding the dynamics of the process. Modeling has always been a complex task due to the complex mechanical flow, thermal transfer and material transformation mechanisms involved in the description of the process [Doumanidis and Kwak, 2001]. Therefore, some authors have restricted themselves to empirical modeling to relate the clad characteristics to the process parameters.

Weerasinghe *et al*. (1983) performed the initial efforts to empirically model the laser cladding process. They concentrated on producing uniform clad layers by overlapping single clad tracks. This work explored the effect of laser power, beam diameter and mode structure, traverse speed, powder flowrate and powder shape and size on cladding rate, clad thickness and width, surface finish, powder utilization, substrate dilution, segregation, porosity, residual stress, cracking, microstructure, and adhesion. The empirical relations based on the experimental results showed the variation of clad width and clad height to the variation in cladding speed, coverage rate, and overlap factor.

Blake *et al*. (1985) explained the effect of irregular powder flowrates on dilution of laser cladding processes. For constant laser power and traverse speed, the amount of powder flowing into the melt pool determines the energy available at the substrate and hence the amount of dilution. Therefore, the less powder fed into the melt zone, the greater the dilution. However, more powder fed into the melt zone results in a significant reduction of specific energy into the substrate, creating a possible lack of fusion. They used a dynamic powder feeder with an in–process feedback control system to determine the affect of powder feeder variables (flowrate, flow orientation, etc.), laser associated variables (power, beam configuration, etc.), and traverse speed of the positioning system on surface finish, dilution, cracking, porosity, homogeneity, adhesion, and distortion.

Hu *et al*. (2001) discussed the instabilities and irreparability problem suffered by SFF methods for metal part building due to the presence of a large number of parameters governing the process. The authors used infrared imaging of the melt pool as an imaging technique for controlling the 3D laser melt pool. Relationships have been established based on the variations of the characteristics of images with variations in the process parameters. A PID controller was designed with feedback from infrared image sensing to control the area of the thermal field. The area of the thermal field represents the laser energy absorbed by the part per unit length in the processing zone. Hence, the control of the area of the thermal field, by regulating laser power and traverse speed, brings an even heat input rate in 3D laser cladding. The authors also demonstrated that, by controlling the heat input during the laser deposition process, the geometrical accuracy, uniformity of deposits, and microstructure can be improved.

Koomsap *et al*. (2001) developed a simulation–based design of a laser–based free–forming process controller. The difficulty in designing a process for the models is the nonlinear effect of individual process parameters in the temperature field (Koomsap *et al*., 2001). The authors developed a metamodel, which is an estimation of the physical model that relates the surface temperature to laser power, table velocity, and powder flowrate. The surface temperature was represented as a function of laser power, table velocity, and powder flowrate. Based on the simulations obtained for different settings of the laser power, table velocity, and powder flowrate, a steady state metamodel was developed using the polynomial regression models from

the steady state results. This was used to form a dynamic metamodel based on the criteria that the surface temperature during the transient periods was non oscillatory, implying the process was either a critically damped or overdamped process.

A novel method of rapid layered manufacturing for building fully–dense metal parts by preplaced powder technique was investigated by Yevko *et al*. (2001). They considered pulsed–laser mode, continuous laser mode, power level, laser beam, and scanning speed as parameters that influenced the clad properties: namely, height and width. A process model was developed and simulated to determine qualitative relationships between process parameters and clad properties by calculating the global temperature field within the powder and baseplate. The nonlinear heat transfer problem was solved by a numerical finite–difference method.

A two–dimensional finite element model for laser cladding by powder injection was developed by Hoadley *et al*. (1992) to study the effect of laser power and processing velocity on the thickness of the deposited clad. This model determines the steady state temperature field, the shape of the melt pool and the position of the melt surface relative to the laser beam. An emperical model for laser cladding was developed by Toyserkani *et al*. (2002) for realtime process control. A Hammerstein–Wiener nonlinear model and a Elman recurrent neural network were implemented to identify the dynamic laser cladding model. The Hammesteine–Wiener approach proved more useful in accurately describing the transient response of the process. Laser intensity, table velocity, and powder feedrate were the inputs, and clad height and melt pool temperature were the process output parameters.

Selective Laser Sintering (SLS) is one of the leading commercial RP technologies that build solid objects by selectively fusing powder at each successive layer according to a numerically–defined cross–sectional geometry. Williams *et al*. (1998) modeled the effects of selected parameters on the SLS process by determining the amount of energy delivered at the substrate surface. A three–dimensional heat diffusion problem was formed to describe the thermal energy transferred in the SLS process.

PROCESS MODELING

A more general dynamic process model for the laser metal deposition process was presented in Doumanidis and Kwak (2001). This model has the capability to form the basis for a process controller. This paper will perform an analysis of this model. First, the model is briefly presented. Performing a mass balance of the melt pool

$$\rho \dot{V}(t) = -\rho A(t) v(t) + \mu_m m(t) \tag{1}$$

where ρ is the material density (kg/m^3) and is assumed to be constant, V is the bead volume (m^3), A is the cross sectional area in the direction of deposition (m^2), v is the table velocity in the direction of deposition (m/s), μ_m is the powder catchment efficiency, and m is the powder flow rate (kg/s). Assuming an elliptical bead, the volume and cross sectional area in the direction of deposition, respectively, are given by

$$V(t) = \frac{\pi}{6} w(t) h(t) l(t) \tag{2}$$

$$A(t) = \frac{\pi}{4} w(t) h(t) \tag{3}$$

where w is the bead width (m), h is the bead height (m), and l is the bead length (m). Performing a momentum balance of the melt pool in the direction of deposition

$$\rho \dot{V}(t) v(t) + \rho V(t) \dot{v}(t) = \rho \frac{\pi}{4} w(t) h(t) v^2(t) + \left[1 - \cos(\theta)\right]\left[\gamma_{GL} - \gamma_{SL}\right] w(t) \tag{4}$$

where θ is the wetting angle (rad), γ_{GL} is the gas to liquid surface tension parameter, and γ_{SL} is the solid to liquid surface tension parameter. Performing an energy balance of the melt pool

$$\begin{aligned} \rho c_l \dot{T}(t) V(t) + \rho \dot{V}(t)\left[c_s\left(T_m - T_0\right) + h_{SL} + c_l\left(T(t) - T_m\right)\right] = -\rho \frac{\pi}{4} w(t) h(t) v(t) c_s\left(T_m - T_0\right) + \\ \mu_Q Q(t) - \frac{\pi}{4} w(t) l(t) \alpha_s\left(T(t) - T_m\right) - \left[\frac{\pi}{\sqrt[3]{2}}\left[w(t) h(t) l(t)\right]^{\frac{2}{3}}\right]\left[\alpha_G\left(T(t) - T_0\right) + \varepsilon\sigma\left(T^4(t) - T_0^4\right)\right] \end{aligned} \tag{5}$$

where T is the average melt pool temperature (K), c_s is the solid material specific heat ($J/(kgK)$), T_m is the melting temperature (K), T_0 is the ambient temperature (K), h_{SL} is the specific latent heat of fusion–solidification (J/kg), c_l is the molten material specific heat ($J/(kgK)$), μ_Q is the laser efficiency, Q is the laser power (W), α_s is the convection coefficient (W/m^2K), α_G is the heat transfer coefficient (W/m^2K), ε is the surface emissivity, and σ is the Stefan–Boltzmann constant (W/m^2K^4). Using the steady–state solution for the conductive temperature distribution in a material subjected to an energy source moving at a constant velocity, the bead width–length relationship at the average temperature is given by the following elliptical relationship

$$l(t) = X(t) + 0.25\frac{w^2(t)}{X(t)} \quad with \quad X(t) = \max\left[\frac{w(t)}{2} \quad \frac{\mu_Q Q(t)}{2\pi k\left(T(t) - T_0\right)}\right] \tag{6}$$

where k is the thermal conductivity constant ($W/(mK)$).

EQUILIBRIUM ANALYSIS

It is often of interest to determine the steady–state solution of equations (1)–(6). Two situations will be considered: one where the process variables are known and the process parameters must be determined and one where the process parameters are known and the process variables must be determine. Often, the designer knows the desired melt pool temperature, bead width, and bead height. Typically the bead length is not of interest. In this case, the designer would like to determine the process parameters that produce the desired melt pool temperature, bead width, and bead height. Setting the left hand side of equation (4) to zero, the equilibrium table velocity is

$$\bar{v} = \sqrt{\frac{-4\left[1-\cos(\theta)\right]\left[\gamma_{GL}-\gamma_{SL}\right]}{\rho\pi\bar{h}}} \tag{7}$$

where the bar denotes equilibrium value. Note that γ_{GL} must be less than γ_{SL} for the equilibrium table velocity to be positive. Setting the left hand side of equation (1) equal to zero, the equilibrium powder flow rate is

$$\bar{m} = \frac{\rho\pi\bar{w}\bar{h}\bar{v}}{4\mu_m} \tag{8}$$

To solve for the equilibrium laser power and the equilibrium bead length, the left hand side of equation (5) is set equal to zero and the bisection routine is applied to the resulting equation and equation (6). Note that if the bead length is equal to the bead width, equation (5) may be directly solved for the equilibrium laser power; however, for many situations this is not the case. Finally, the equilibrium bead volume is solved using equation (2).

The following parameters are taken from Doumanidis and Kwak (2001): ρ = 7200 kg/m^3, μ_m = 0.92, μ_Q = 0.58, T_0 = 292 K, $\theta = 90^0$, c_l = 780 $J/(kgK)$, $h_{SL} = 2.45*10^5$ J/kg, T_m = 1673 K, α_s = 183 $W/(m^2K)$, $\sigma = 5.67*10^{-8}$ $W/(m^2K^4)$, α_G = 24 $W/(m^2K)$, and ε = 0.53. To achieve the same simulation results presented in Doumanidis and Kwak (2001), the following parameters were found by trial and error: k = 6.5 $W/(mK)$, $\gamma_{GL}-\gamma_{SL}$ = –0.00036, and c_s = 1250 $J/(kgK)$. For a desired melt pool temperature of 2000 K, bead width of 5 mm, and bead height of 2 mm, the powder flow rate, table velocity, and laser power should be 20.8 g/min, 5.64 mm/s, and 999 W, respectively. Also, the bead length and volume, respectively, are 9.06 mm and 47.4 mm^3.

Sometimes a designer would like to predict the melt pool temperature and bead morphology for a set of process parameters. Given, the powder flow rate, laser power, and table velocity, equations (1)–(6) are solved for the melt pool temperature and bead morphology. Setting the left hand side of equation (4) to zero, the equilibrium bead height is

$$\bar{h} = \frac{-4\left[1-\cos(\theta)\right]\left[\gamma_{GL}-\gamma_{SL}\right]}{\rho\pi\bar{v}^2} \tag{9}$$

Again, note that γ_{GL} must be less than γ_{SL} for the equilibrium bead height to be positive. Setting the left hand side of equation (1) equal to zero, the equilibrium bead width is

$$\bar{w} = \frac{4\mu_m\bar{m}}{\rho\pi\bar{h}\bar{v}} \tag{10}$$

To solve for the equilibrium melt pool temperature and the equilibrium bead length, the left hand side of equation (5) is set equal to zero and the bisection routine is applied to the resulting equation and equation (6). Finally, the equilibrium bead volume is solved using equation (2). For a powder flow rate, table velocity, and laser power of 25 g/min, 5 mm/s, and 1200 W,

respectively, the melt pool temperature is 1928 *K*, the bead width is 5.32 *mm*, the bead height is 2.55 *mm*, the bead length is 11.1 *mm*, and the bead volume is 78.8 mm^3.

The equilibrium bead height is inversely proportional to the square of the table velocity and is independent of the other process parameters. The equilibrium bead width is proportional to the powder flow rate, proportional to the table velocity, and is independent of the laser power. The melt pool temperature and bead length depend on all of the process parameters. The sensitivities of melt pool temperature and bead length with respect to laser power, table velocity, and powder flow rate are shown in Figure 1 for the numerical parameters given above. For sensitivities with respect to laser power, the powder flow rate and table velocity are 25 *g*/*min* and 5 *mm*/*s*, respectively. For sensitivities with respect to powder flow rate, laser power and table velocity are 1200 *W* and 5 *mm*/*s*, respectively. For sensitivities with respect to table velocity, the laser power and powder flow rate are 1200 *W* and 25 *g*/*min*, respectively. The melt pool temperature is relatively constant for low laser powers, increases quickly for laser powers around 1100–1200 *W*, and increases slowly for high laser powers. For the laser metal deposition process, it is desirable to keep the melt pool temperature just above the melting temperature; in this example, 1750–1850 *K*. If the melt pool temperature is too low, the substrate and powder will not melt and, if the melt pool temperature is too high, plasma will result and the part microstructure will not form properly. The bead length is minimum around 1100–1200 *W*, increases quickly for low laser powers, and increases slowly for high laser powers. For a very low laser power, approximately 200 *W*, both the melt pool temperature and bead length suddenly become small. This is due to the discontinuity in equation (6). The laser power becomes so small that the bead length is equal to the bead width. The melt pool temperature is a maximum for a table velocity of approximately 10 *mm*/*s*, decreases sharply for lower table velocities, and decreases slowly for higher table velocities, eventually becoming constant. The bead length is a minimum for a table velocity of approximately 5 *mm*/*s* and increases sharply for lower and higher table velocities. The melt pool temperature is relatively constant for high powder flow rates and increases steadily as the powder flow rate decreases. The bead length increases slowly as the powder flow rate increases until approximately 25 *g*/*min* where the bead length increases sharply. From a controls perspective, it appears that table velocity, powder flow rate, and laser power should be used to regulate bead height, bead width, and melt pool temperature, respectively.

SIMULATION STUDIES

A series of simulations are now conducted to analyze the laser metal deposition system. To simulate the differential–algebraic equations, a 4^{th} order Runge–Kutta routine is used. An initial bead volume and an initial melt pool temperature are specified. Given initial conditions for the process parameters, equations (2), (4), and (6) are solved iteratively to determine consistent conditions for the bead dimensions (i.e., width, height, and length). The differential equations (1) and (5) are solved at each time step using the 4^{th} order Runge–Kutta routine and equations (2), (4), and (6) are solved iteratively to determine the bead dimensions. Note that the 4^{th} order Runge–Kutta routine requires intermediate derivative calculations that, in turn, require intermediate values of the state and algebraic variables. Thus, for every intermediate bead volume and melt pool temperature values, the bead dimensions are solved iteratively using equations (2), (4), and (6).

Simulations for step changes in the process parameters are shown in Figure 2. The system operates under steady conditions for 5 seconds and then the step changes in the process parameters are applied. The laser power changes from 1200 *W* to 1440 *W*, the table velocity changes from 5 *mm*/*s* to 6 *mm*/*s*, and the powder flow rate changes from 25 *g*/*min* to 30 *g*/*min*. The time responses were first–order and second–order type responses. It is interesting to note that the melt pool temperature had a smooth response while the bead dimensions, which are governed by the algebraic equations, had sharp responses to step changes in the process variables. Also, a step change in powder flow rate alone caused a very slow response in the bead dimensions as compared to the other simulations. To understand the stability characteristics, a multitude of simulations are conducted and the phase plots, i.e., plots of a state variable versus another state variable, are graphed. The phase plots are shown in Figure 3 for a variety of process parameter combinations. The phase plots include bead volume versus melt pool temperature, bead width versus bead height, bead width versus bead length, and bead height versus bead length. In all of the phase plots, the trajectories go to the equilibrium parameter values demonstrating the system is stable in the given region. It is interesting to note that the bead width and bead height have an inverse relationship.

SUMMARY, CONCLUSIONS, AND FUTURE WORK

This paper analyzed the equilibrium and stability properties of a dynamic model of the laser metal deposition process. The equilibrium bead height is inversely proportional to the table velocity and the equilibrium bead width is proportional to the powder flow rate and table velocity. The equilibrium bead length and melt pool temperature have a complex relationship to all of the process parameters. The dynamic analysis showed that the equilibrium is a stable equilibrium with a large region of attraction. Also, the bead width and bead height dynamically have an inverse relationship. In future work, analytically approximations of the sensitivity of the equilibrium bead length and equilibrium melt pool temperature to the process parameters and the region of attraction will be determined.

ACKNOWLEDGEMENTS

The authors gratefully acknowledge the financial support of the National Science Foundation (DMI–9871185), Society of Manufacturing Engineers (#02022–A), Missouri Research Board, and UMR's Intelligent Systems Center.

REFERENCES

Blake, A.G. and Eboo, G.M., 1985, "State of the Art Laser Hardfacing Using Dynamic Powder Feed Technology," *Conference on the Laser vs. the Electron Beam in Welding, Cutting and Surface Treatment*, Reno, Nevada, pp. 196–214.

Boddu, M.R., Landers, R.G., and Liou, F.W., 2001, "Control of Laser Cladding for Rapid Prototyping–A Review," *Twelfth Annual Solid Freeform Fabrication Symposium*, Austin, Texas, August 7–9, pp. 460–467.

Doumanidis, C. and Kwak, Y.M., 2001, "Geometry Modeling and Control by Infrared and Laser Sensing in Thermal Manufacturing with Material Deposition," *ASME Journal of Manufacturing Science and Engineering,* Vol. 123, pp. 45–52.

Hu, D., and Wu, Y., 2001 "Heat Input Control in 3D Laser Cladding Based on Infrared Sensing," *ASME International Mechanical Engineering Congress and Exposition*, November, pp. 333–341.

Hoadley, A.F.A. and Rappaz, M., 1992, "A Thermal Model of Laser Cladding by Powder Injection," *Metallurgical Transactions Part B*, Vol. 23B, pp. 631–642.

Eager, T.W., and Tsai, N.S., 1983, "Temperature Fields Produced by Traveling Distributed Heat Sources," *Welding Journal*, Vol. 62, No. 12, pp. 346s–355s.

Koomsap, P., Prabhu, V.V., Schriempf, J.T., and Reutzel, E.W., 2001, "Simulation–Based Design of Laser–Based Free Forming Process Control," *Journal of Laser Applications*, Vol. 13, No. 2, pp. 47–59.

Steen, W.M., 1998, *Laser Material Processing*, 2nd Edition, Springer Verlag.

Toyserkani, E., Khajepour, A., and Corbin, S., 2002, "Application of Experimental–Based Modeling to Laser Cladding," *Journal of Laser Applications*, Vol. 14, No. 3, pp. 165–173.

Weerasinghe, V.M. and Steen, W.M., 1983, "Laser Cladding with Pneumatic Powder Delivery," *Lasers in Materials Processing*, pp. 166–174.

Williams, J.D. and Deckard, C.R., 1998, "Advances in Modeling the Effects of Selected Parameters on the SLS Process," *Rapid Prototyping Journal*, Vol. 4, No. 2, pp. 90–100.

Yevko, V., Park, C.B., Zak, G., Coyle, T.W., and Behabib, B., 1998, "Cladding Formation in Laser Beam Fusion of Metal Powder," *Rapid Prototyping Journal*, Vol. 4, No. 4, pp. 168–184.

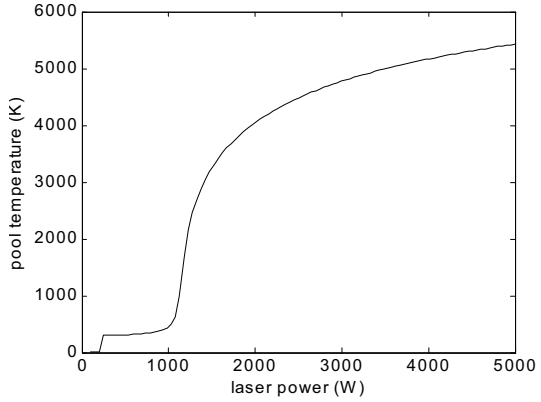

(a) melt pool temperature vs. laser power

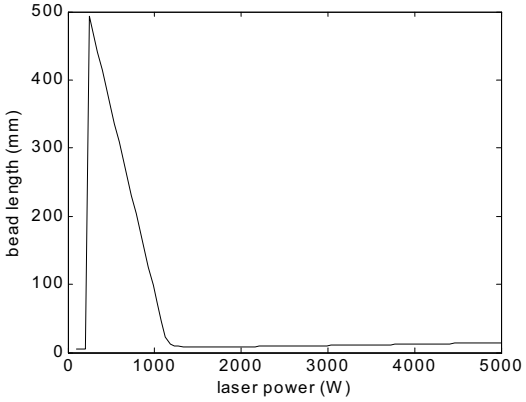

(b) bead length vs. laser power

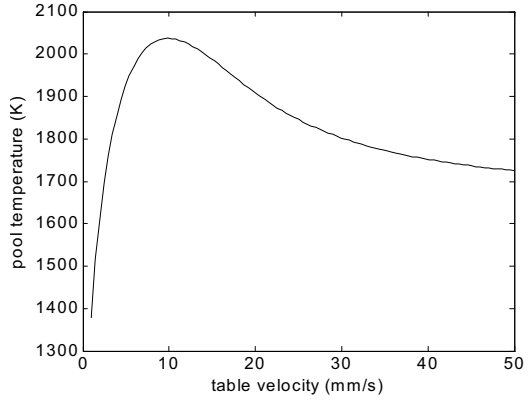

(c) melt pool temperature vs. table velocity

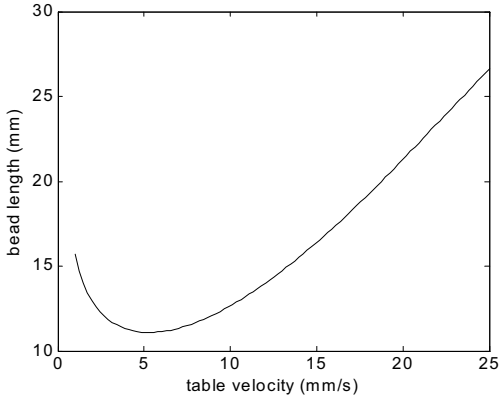

(d) bead length vs. table velocity

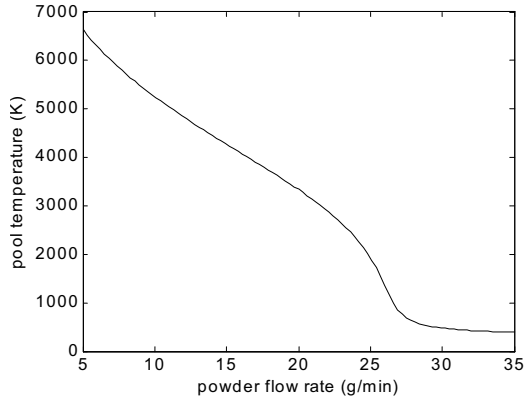

(e) melt pool temperature vs. powder flow rate

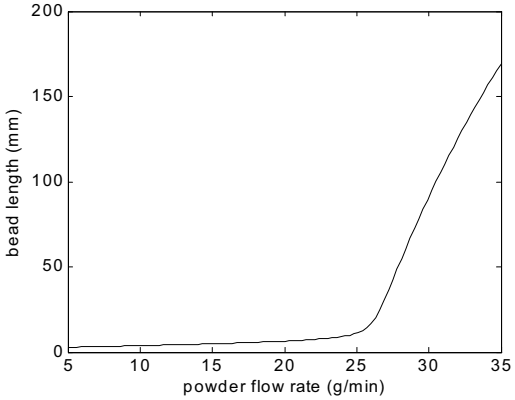

(f) bead length vs. powder flow rate

Figure 1: Equilibrium Melt Pool Temperature and Bead Length as a function of Process Parameters.

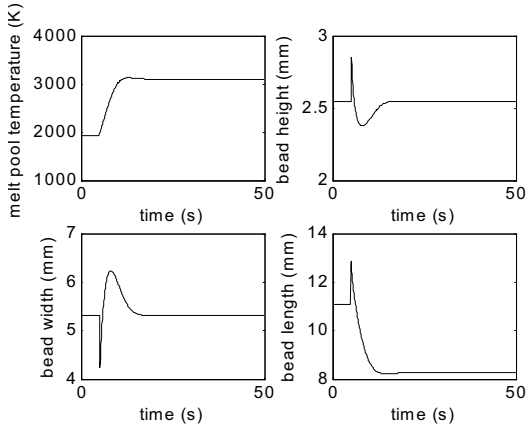

(a) step change in laser power

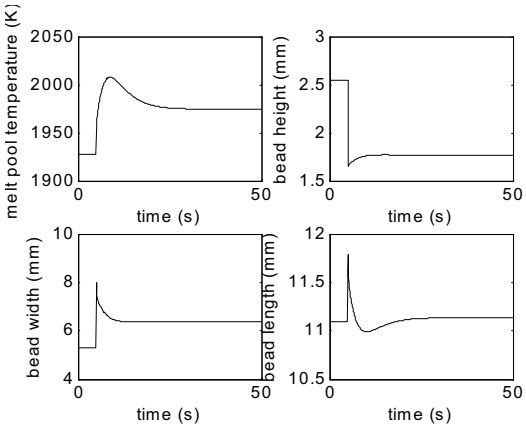

(b) step change in table velocity

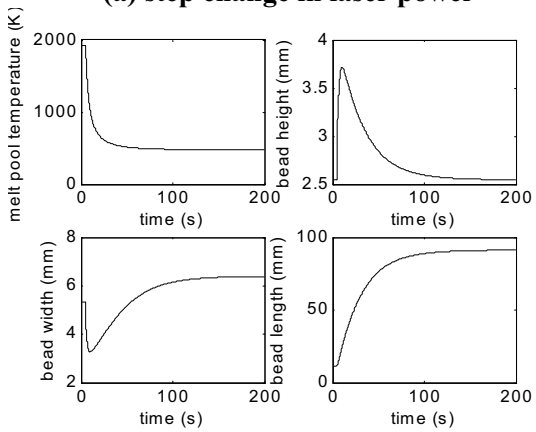

(c) step change in powder flow rate

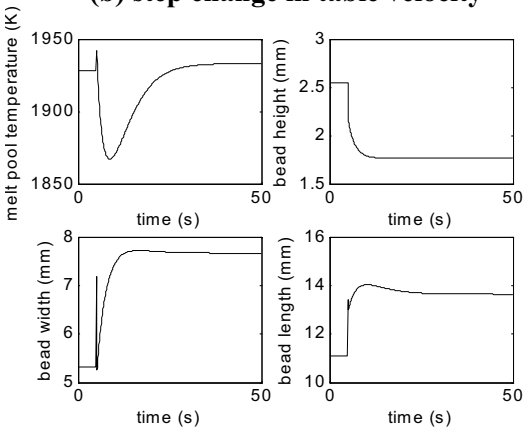

(d) step change in all process parameters

Figure 2: Dynamic Simulation with $Q(0) = 1200$ W, $v(0) = 5$ mm/s, $m(0) = 25$ g/min, $V(0) = 78.8$ mm^3, $T(0) = 1930$ K, $w(0) = 5.32$ mm, $h(0) = 2.55$ mm, and $l(0) = 11.1$ mm.

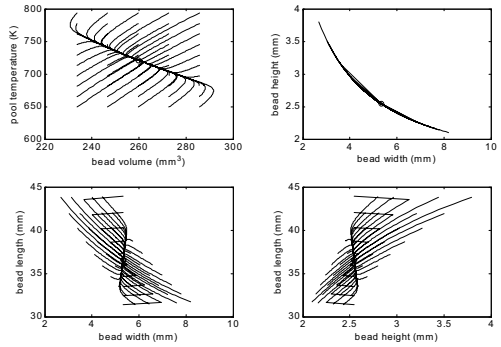

(a) Q = 1100 W, m = 25 g/min, and v = 5 mm/s

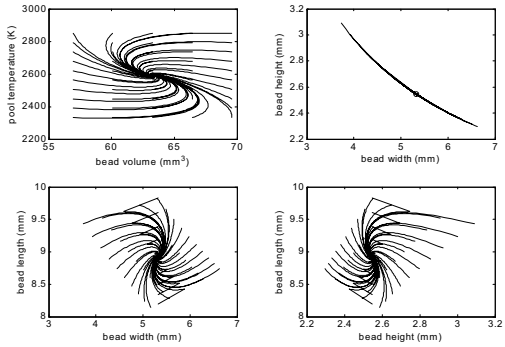

(b) Q = 1300 W, m = 25 g/min, and v = 5 mm/s

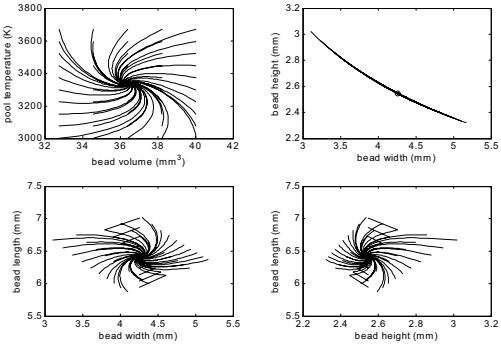

(c) Q = 1200 W, m = 20 g/min, and v = 5 mm/s

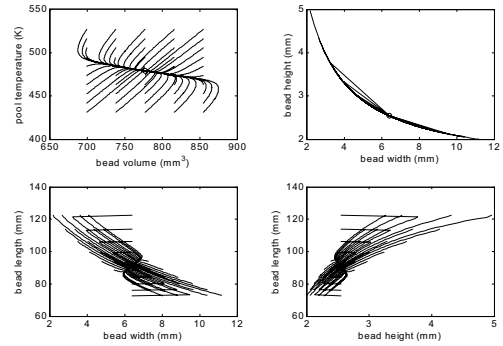

(d) Q = 1200 W, m = 30 g/min, and v = 5 mm/s

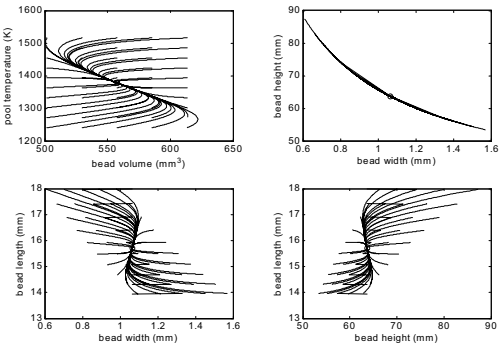

(e) Q = 1200 W, m = 25 g/min, and v = 1 mm/s

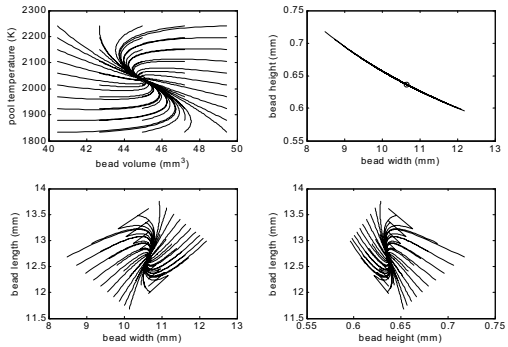

(f) Q = 1200 W, m = 25 g/min, and v = 10 mm/s

Figure 3: Phase Plots. Equilibrium Point Denoted by Circle.